Chinese Journal of
POLYMER SCIENCE

RESEARCH ARTICLE

https://doi.org/10.1007/s10118-026-3679-5
Chinese J. Polym. Sci. **2026**, *44*, 2607–2618

Recyclable and Easy-to-apply Amidoxime Functionalized Cellulose for Continuous Removal of Iron Ions from Shipwreck Woods

Ting-Ting Zhang[a,d], Hong-Ying Zhang[c], Hong-Liang Kang[a*], Da-Wa Shen[b], and Rui-Gang Liu[a,d*]

[a] *Laboratory of Polymer Physics and Chemistry, Beijing National Laboratory of Molecular Sciences, Institute of Chemistry, Chinese Academy of Sciences, Beijing 100190, China*
[b] *China Academy of Cultural Heritage, Beijing 100029, China*
[c] *School of Conservation Science & Technology for Cultural Heritage, Key Laboratory of Materials and Technology for Unearthed Cultural Heritage Conservation, Shaanxi University of Science & Technology, Xi'an 710021, China*
[d] *University of Chinese Academy of Sciences, Beijing 100049, China*

Electronic Supplementary Information

Abstract Amidoxime functionalized gauze (Ami-gauze) was prepared by a simple finishing process, in which the gauze was immersed in amidoxime cellulose and crosslinker solution and then dried. Ami-gauze has been used as an adsorbent for the conservation of marine wooden cultural relics to adapt to their irregular surfaces. This material capitalizes on the synergistic interaction between the hygroscopic properties of gauze and the metal-binding affinity of functional polymers, achieving superior efficiency in removing iron ions from degraded wooden artifacts. Notably, the composite retained more than 87.6% of its adsorption capacity after nine regeneration cycles through simple aqueous immersion, highlighting its operational simplicity and reusability. The cellulose-based adsorbent is cheap and scalable, which presents a promising solution for mitigating iron-induced degradation in marine archaeological artifacts.

Keywords Cellulose; Amidoxime functionalization; Adsorption; Wooden cultural relics; Conservation

Citation: Zhang, T. T.; Zhang, H. Y.; Kang, H. L.; Shen, D. W.; Liu, R. G. Recyclable and easy-to-apply amidoxime functionalized cellulose for continuous removal of iron ions from shipwreck woods. *Chinese J. Polym. Sci.* **2026**, *44*, 2607–2618.

INTRODUCTION

The iron-induced degradation of archaeological waterlogged wood is a critical challenge for heritage conservation.[1–3] The redox cycling of Fe(II)/Fe(III) catalyzes the degradation of archaeological waterlogged wood, leading to a catastrophic loss of mechanical strength within decades of excavation. The composition of iron compounds, including iron sulfides, iron oxides, and iron salts,[4–7] varies according to the burial environment and oxygen exposure of the archaeological waterlogged wood. Currently, the primary treatment involves bulk chelation baths with oxidants and chelating agents as well as their combinations or sequential applications.[8,9] Typical oxidants include sodium persulfate ($Na_2S_2O_8$) and hydrogen peroxide (H_2O_2). Effective chelating agents contain diethylenetriamine pentaacetic acid (DTPA), ethylenediaminetetraacetic acid disodium (EDTA-2Na), ammonium citrate, and oxalic acid.[9] However, the immersion method has limitations of poor penetration depth and secondary precipitation of Fe-chelator complexes within the wood matrix. A controllable, noninvasive extraction strategy to avoid secondary contamination is preferred. Adsorbent materials could be another choice for removing iron ions from archaeological waterlogged wood. The key issue is to fabricate adsorbent materials in suitable forms with easy operation, high efficiency, and good reusability.

In a previous study, we designed and synthesized a water-soluble amidoxime cellulose complexing agent inspired by biological systems (ISIP1 and Mfp-5). This agent utilizes specific binding sites for high-affinity iron capture, effectively removing iron deposits from archaeological waterlogged wood in aqueous baths.[10] However, the cellulose-based complexing agents are used in aqueous media, resulting in secondary precipitation. To address this issue, we propose a transition from passive liquid immersion to active solid-phase extraction. Cellulose, a renewable and non-toxic natural polymer,[11] can be functionalized *via* derivatization or graft copolymerization for different applications.[12–17] Its intrinsic structural homology with archaeological wood promotes interfacial hydrogen bonding and ensures a stable, cohesive interface with waterlogged timber, thereby minimizing the delamination risks associated with heterologous materials.

In this work, the water-soluble amidoxime cellulose was immobilized *via* a finishing approach to fabricate soft-solid phase adsorbent materials that provide mechanical conformability, allowing its conformal application on the surface

* Corresponding authors, E-mail: hlkang@iccas.ac.cn (H.L.K.)
E-mail: rgliu@iccas.ac.cn (R.G.L.)
Received February 5, 2026; Accepted March 18, 2026; Published online July 1, 2026

of archaeological wood with complex topologies to remove iron ions. The amidoxime groups with *O, N*-bidentate cavities provide sites for iron binding, while the textile structure allows for easy removal and reusability after washing with EDTA solution. This design effectively solves the problem of secondary precipitation by physically separating the captured iron from the wood. The adsorption mechanism of Ami-gauze on Fe(III) was investigated in detail. The kinetic results demonstrated a chemisorption-dominated adsorption mechanism. Isotherm analysis revealed that the adsorption process involves heterogeneous surface interactions and multilayer adsorption. The material can be recovered *via* immersion in an EDTA-2Na solution to desorb adsorbed iron ions. Amidoxime functionalized cellulose materials show promising applications for removing iron deposits from the marine archaeological wood.

EXPERIMENTAL

Materials

Amidoxime cellulose (AOC) was synthesized according to our previous work, with a degree of polymerization of 150 and a degree of amidoxime group substitution of 1.78.[18] Medical gauze (21 s × 32 s) was supplied by Hualu Sanitary Materials (Shandong, China). Polyurethane-based crosslinking agent (PCL, solid content of 33%) was purchased from Jiubang Chemical (Shanghai, China). Ethylenediaminetetraacetic acid disodium dihydrate (EDTA-2Na, 99%), $FeCl_3{\cdot}6H_2O$ (97%), HCl (35%), CH_3COOH, and NaOH were of AR grade and purchased from local chemical suppliers.

Marine archaeological wood was sampled from the Nanhai I shipwreck, a loose timber used to secure cargo on cargo ships (Fig. 1). The iron deposits include pyrite (FeS_2), siderite ($FeCO_3$), goethite (FeOOH), and magnetite (Fe_3O_4) at varying concentrations.[19]

Fig. 1 Loose wood from Nanhai I shipwreck.

Preparation of Amidoxime Cellulose Modified Gauze

The medical gauze was desized before use. It was then immersed in an aqueous solution of NaOH (35 wt%) at 45 °C for 40 min, followed by transferring it into HCl (5 wt%)/CH_3COOH (6 wt%) mixing solution for 40 min. Then, the samples were thoroughly washed with deionized water and dried at 75 °C for 30 min to obtain desized gauze (De-gauze).

Amidoxime functionalized gauze (Ami-gauze) was prepared by finishing. AOC (10.0 g·L^{-1}) and PCL (3.2 g·L^{-1}) solutions were first prepared. De-gauze (50.0 g) was immersed in a 1.0 L finishing solution for 1.0 h to ensure thorough infiltration. The gauze was removed, squeezed to remove excess finishing solution, and oven-dried at 120 °C for 5 min to obtain Ami-gauze. The bulk mass loading[20] of the AOC was determined to be 1.24 wt%, calculated by:

$$\text{AOC content (\%)} = \frac{m_{\text{Ami}} - m_{\text{De}}}{m_{\text{Ami}}} \times \frac{1}{1 + c_{\text{PCL}}/c_{\text{AOC}}} \times 100\% \quad (1)$$

where m_{Ami} and m_{De} are the masses of the Ami- and De-gauze, respectively; c_{PCL} and c_{AOC} are the concentrations of AOC and PCL in the finishing solution, respectively.

Adsorption of Fe(III) Ions of Ami-gauze

Ami-gauze (1.0 g) was immersed in a 250 mL of $FeCl_3$ aqueous solution (5.6–139.1 mg·L^{-1}) with stirring at 25 °C. The Fe(III) concentration in the solution was determined by withdrawing 3 mL of the solution at the desired intervals. Three parallel experiments were performed to ensure reproducibility. The adsorption capacity and removal efficiency were calculated as follows Eqs. (2) and (3):

$$Q_t = \frac{(c_0 - c_t)V}{m} \quad (2)$$

$$Q_e = \frac{(c_0 - c_e)V}{m} \quad (3)$$

where c_0, c_t, and c_e are the Fe(III) concentrations (mg·L^{-1}) at $t = 0$, time t, and equilibrium state, respectively, when using Ami-gauze with a mass of m (g) in a $FeCl_3$ solution of V (L). Q_t and Q_e (mg·g^{-1}) are the Fe(III) ions adsorbed by the Ami-gauze at t and equilibrium states, respectively.

The color strength (*K/S*) of Ami-gauze was determined using the Kubelka-Munk theory,[21]

$$K/S = \frac{(1 - R)^2}{2R} \quad (4)$$

where R is the reflectance at the wavelength of maximum adsorption, K is the adsorption coefficient, and S is the scattering coefficient. The *K/S* value increases with the color depth.

The reusability of the Ami-gauze was estimated *via* cyclic adsorption-desorption experiments. Adsorption was achieved by immersing the Ami-gauze (0.08 g) in 20 mL of $FeCl_3$ solution (20 mg·L^{-1}) with continuous stirring for 24 h at room temperature. The adsorption capacity of the Ami-gauze was estimated by measuring the concentration of Fe(III) in the solution. Desorption was performed by immersing the Fe(III) adsorbed Ami-gauze in 100 mL of saturated EDTA-2Na solution (replaced every 6 h) and stirring for 24 h at room temperature, followed by rinsing in deionized water to reactivate the Ami-gauze.

Removing Iron Ions from Marine Archaeological Wood with Ami-gauze

The archaeological wood samples were immersed in deionized water at room temperature. Seven pieces of Ami-gauze (about 0.05 g and 3 cm × 3 cm) were attached to the wood surface where iron deposits were relatively uniformly distributed. The Ami-gauze was removed from the wood surface at the desired time and immersed in 100 mL of EDTA-2Na solution (10 mmol·L^{-1}) for 50 h to desorb Fe(III) ions bound to the Ami-gauze. Subsequently, the Ami-gauze was rinsed with deionized water and reattached to the wood surface to continue the ex-

https://doi.org/10.1007/s10118-026-3679-5

traction process. This procedure was repeated eight times.

Application of Ami-gauze to Remove Iron Deposits from the Hull of Nanhai I Shipwreck

The effectiveness of Ami-gauze was determined as follows. Two pieces of Ami-gauze with similar weights and dimensions were attached to the bulkhead surface of the Nanhai I shipwreck, which exhibited significant iron deposits. The samples were stapled using bamboo nails to prevent detachment. After adsorption for a certain period, the samples were peeled from the archaeological wood, washed with deionized water, and further squeezed to remove excess water. Then, both samples were immersed in an excess EDTA-2Na solution for 6 h to desorb the adsorbed Fe(III) ions under ultrasonication. The samples were squeezed after desorption. The washing water and EDTA-2Na solution were collected to quantify the iron content by ICP analysis. Adsorption efficiency (E_a) is calculated by the following equation (Eq. 5):

$$E_a = \frac{W_i}{W_g} \quad (5)$$

where W_i and W_g are the masses of iron adsorbed from wood and gauze, respectively. Adsorption-desorption cycles were performed under the same conditions to estimate the reusability.

Characterizations

Fourier transform infrared (FTIR) spectra were collected on a Bruker Tensor 27 instrument in the attenuated total reflection (ATR) mode over the range of 4000–600 cm^{-1} at a resolution of 4 cm^{-1} for 64 scans. Color strength (*K/S*) of Ami-gauze was measured on a Datacolor 800 spectrophotometer (Datacolor AG, Switzerland) with a D_{65} illuminant and a 10° standard observer with the specular component included (SCI) mode. The Fe(III) ions concentration in the solution was measured using an inductively coupled plasma atomic emission spectrometer (Agilent 5800 VDV ICP-OES, USA) at 238.2 nm. Surface morphologies of the samples were observed using a scanning electron microscope (SEM, Quanta FEG250, FEI, USA) operating at an accelerating voltage of 3.0 kV. The samples were Pt-coated on an SCD 500 ion sputter coater working at 20 mA for 120 s before the SEM observation. Energy-dispersive spectrometry (EDS) was used to characterize the elements on the surface of the samples using INCAX-sight (Oxford Instruments, UK). X-ray photoelectron spectroscopy (XPS) was performed using an ESCALAB250XI spectrometer (Thermo Fisher Scientific, USA) with a monochromatic Al K*α* source at 1486.6 eV. The XPS survey spectra were recorded at a step of 1 eV and a pass energy of 100 eV. XPS high-resolution spectra of C_{1s}, O_{1s}, N_{1s}, and Fe_{2p} regions were recorded at a step of 0.05 eV and a pass energy of 20 eV for five scans. XPS data were fitted with Avantage software using a two-component Gaussian-Lorentzian sum function to obtain the fine XPS information for N_{1s}, O_{1s}, and C_{1s}.

RESULTS AND DISCUSSION

Static Adsorption and Desorption

The Ami- and control De-gauze, both white in color with *K/S* values of 0.020 and 0.018, respectively, were immersed in the $FeCl_3$ solution. Ami-gauze became yellow after 2 h (Fig. S1a in the electronic supplementary information, ESI), while De-gauze remained slightly yellow during the experimental period (Fig. S1b in ESI). After immersion for 24 h, both the samples were washed with deionized water *via* ultrasonication to eliminate the influence of non-specific physical adsorption. The Ami-gauze is yellow (*K/S*=0.948, Fig. S1e in ESI), and the De-gauze became off-white (*K/S*=0.050) (Fig. S1e in ESI). The results confirm the efficient adsorption of Fe(III) ions on the Ami-gauze and the negligible adsorption of Fe(III) ions on the De-gauze. The adsorbed Fe(III) on the Ami-gauze can be desorbed using a saturated EDTA-2Na solution at room temperature (Fig. S1c in ESI). After 24 h, the Ami-gauze significantly faded to a white state (*K/S*=0.034). Reactivity characteristics are significant for coordination compounds in practical applications.[22,23] SEM micrographs of the Ami-gauze after Fe(III) adsorption (Ami-gauze/Fe) indicate a notable increase in the surface roughness of the gauze fibers along with the presence of particulate deposits, which confirms the binding of Fe(III) upon adsorption (Figs. S2a–S2c in ESI). Correspondingly, EDS analysis confirms the presence of Fe, C, and O elements on the surface of the Ami-gauze/Fe, with the iron content accounting for approximately 0.4% of the total elements (Fig. S2d in ESI). These results suggest that chemisorption rather than simple physical entrapment occurred for adsorption[24] and the potential reusability of Ami-gauze for the adsorption of iron ions.

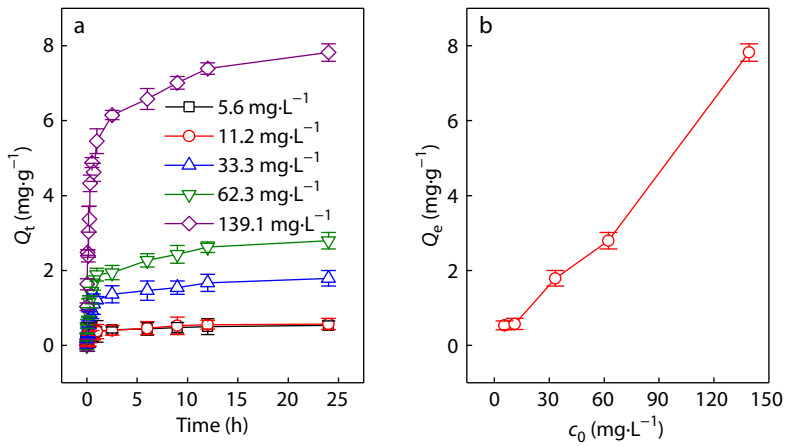

Fig. 2 Fe(III) uptake (Q_t) versus time (a), and the equilibrium metal uptake for Fe(III) (b) with various initial concentrations from 5.6 mg·L^{-1} to 139.1 mg·L^{-1} at 25 °C.

Fig. 2(a) shows the uptake of Fe(III) ions in $FeCl_3$ solutions of different concentrations. The results show typical biphasic kinetics, characterized by an initial rapid uptake phase followed by a gradual approach to equilibrium adsorption behavior.[25,26] The sufficient number of unoccupied active sites on the surface of the adsorbent at the initial stage results in the rapid attachment of adsorbate molecules, followed by a decline in the adsorption rate with the occupation of the active sites until the equilibrium state is reached. Additionally, the equilibrium adsorption capacity of Fe(III) ions was proportional to the initial concentration (Fig. 2b). The equilibrium adsorption capacity increased from 0.53 mg·g^{-1} to 7.82 mg·g^{-1} as the initial concentration rose from 5.6 mg·L^{-1} to 139.1 mg·L^{-1}, which is similar to those of biomass-based adsorbents.[27] At lower initial concentrations, the limited probability of interaction between the adsorbate molecules and active sites resulted in reduced equilibrium adsorption capacities. With an increase in the initial concentration, the enhanced mass transfer driving force promoted more frequent collisions between the adsorbate molecules and active sites, leading to a proportional increase in the equilibrium adsorption capacity.

The isothermal adsorption relates to the adsorbate concentration in the bulk and the adsorbed amount at the interface is generally depicted by the Langmuir, Freundlich, and Temkin models for the adsorption of a single metal ion. These models illustrate the adsorption mechanism based on the theoretical assumptions inherent to each model[28] and the amount of adsorbent required for the adsorption of a quantitative adsorbate. The Langmuir model[29] depicts the adsorption on a homogeneous adsorbent surface, where all sites possess equivalent energy and each site is occupied by only one adsorbate molecule. This model is expressed as Eq. (6).

$$\frac{c_e}{Q_e} = \frac{c_e}{Q_s} + \frac{1}{Q_s K_L} \tag{6}$$

where c_e is the adsorbate concentration in the solution at equilibrium, K_L is the Langmuir adsorption constant, Q_e is the equilibrium adsorbate uptake, and Q_s is the maximum adsorbate uptake by the adsorbent (adsorption capacity). Q_s and K_L can be determined from the slope and intercept of the plot of c_e/Q_e versus c_e, respectively.

The Temkin model considers the effect of decreasing adsorption heat with the coverage of the adsorbent and the adsorbate-adsorbent interaction, which is suitable for systems with varying adsorption heat during the adsorption process. The Temkin model[30] is expressed as Eq. (7).

$$Q_e = \frac{RT}{b}\ln(ac_e) \tag{7}$$

where R is the gas constant, and T is the absolute temperature (K). Constants a and b can be determined by plotting Q_e versus $\ln c_e$.

The Freundlich model[31] depicts the adsorption process on heterogeneous surfaces or the coexistence of multiple adsorption mechanisms, and can be expressed as Eq. (8).

$$\lg Q_e = \lg K_F + \frac{1}{n}\lg c_e \tag{8}$$

where the constant K_F correlates to the adsorbent capacity, and the adsorption intensity $1/n$ corresponds to the nonlinearity of the adsorbate in the solution of equilibrium concentration and those adsorbed on the adsorbent. Plotting of $\lg Q_e$-$\lg c_e$ results K_F and $1/n$. Q_e can be obtained by the Temkin model. $n > 1$ represents favorable adsorption conditions.

Fig. 3 shows the fitting of the experimental data by Langmuir, Temkin, and Freundlich isothermal models. The results indicate that the Freundlich isothermal model demonstrates a better fit for the adsorption of Fe(III) by the Ami-gauze. The parameters K_F = 0.134 and n = 1.242 (n>1) indicate favorable adsorption of Fe(III) ions. This phenomenon is attributed to the heterogeneity of the material surface, variations in the adsorption intensity, and potential for multilayer adsorption, which fundamentally explains the profound failure of the Langmuir model (R^2=0.009). The irregular distribution of amidoxime groups on the surface and the inherent porous structure of the Ami-gauze facilitate the uptake of Fe(III) ions *via* both surface binding and internal pores, enabling multilayer adsorption. The available binding sites are depleted with the gradual occupation of the surface active sites, thus increasing the difficulty of subsequent adsorption events.

Adsorption Kinetics

In order to elucidate the mass transfer rates and specific reaction mechanisms governing the adsorption process, pseudo-first/second-order kinetic models were used to analyze the adsorption kinetics. For the pseudo-first-order kinetic model,[32] the equation is expressed as Eq. (9).

$$\ln(Q_e - Q_t) = \ln Q_e - K_1 t \tag{9}$$

where Q_e and Q_t represent the adsorption capacity at equilibrium and time t, respectively, and K_1 is the rate constant. Plotting $\ln(Q_e - Q_t)$ versus t results Q_e and K_1. As illustrated in Fig. 4(a), the adsorption kinetics of Fe(III) on the Ami-gauze did not follow the

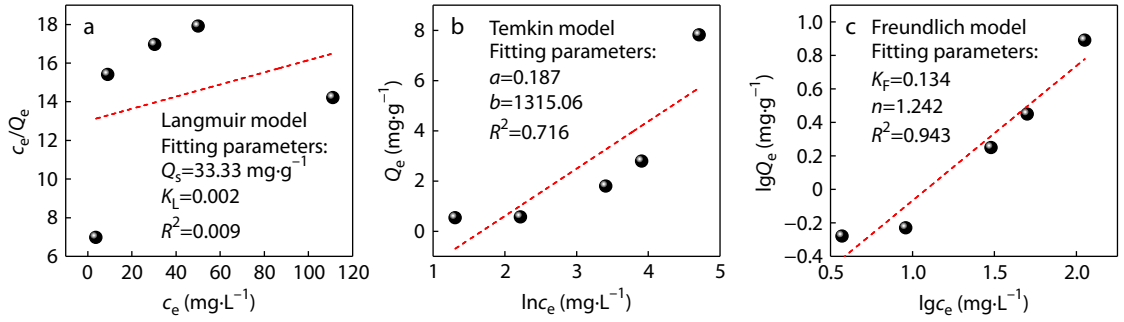

Fig. 3 Fitting of experimental data by (a) Langmuir, (b) Temkin, and (c) Freundlich isothermal models for the adsorption of Fe(III) on Ami-gauze at 25 °C.

https://doi.org/10.1007/s10118-026-3679-5

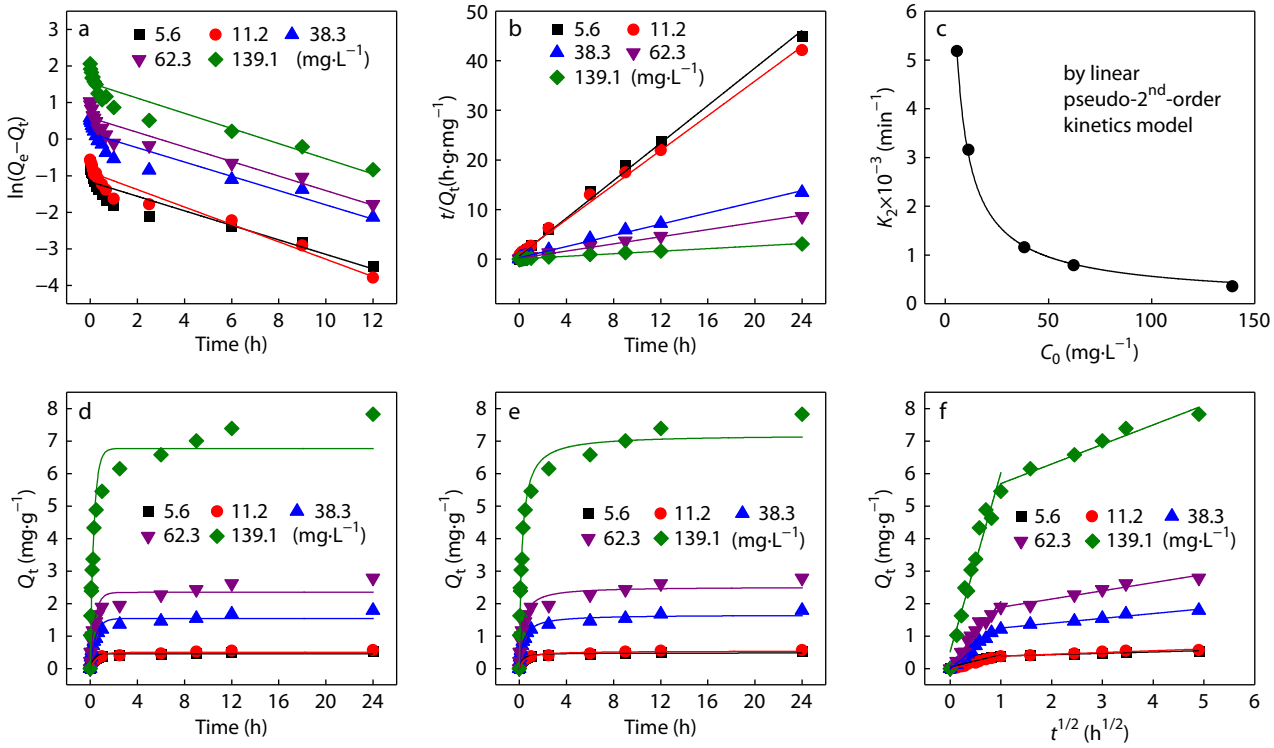

Fig. 4 Linear (a) pseudo-first-order, (b) pseudo-second-order kinetics, (c) variation of the linear second-order rate constant (K_2) with the initial concentration (c_0), (d) nonlinear pseudo-first-order, (e) nonlinear pseudo-second-order kinetics, and (f) intra-particle diffusion kinetics fitting curve for Fe(III) adsorbed on Ami-gauze (T = 25 °C).

pseudo-first-order kinetic model, especially during the initial stage. In contrast, the experimental data can be accurately described by the pseudo-second-order kinetic model (Eq. 10).[33]

$$\frac{t}{Q_t} = \frac{t}{Q_e} + \frac{1}{K_2 Q_e^2} \tag{10}$$

The constants K_2 and Q_e were obtained by plotting t/Q_t versus t (Fig. 4b). The experimental data can be described well using a pseudo-second-order kinetic model. The coefficient of determination (R^2) approached unity for all datasets, and the calculated Q_e was close to the experimental data (Table S1 in ESI). The pseudo-second-order kinetic model emphasizes the strong chemical interactions between the adsorbent and adsorbate. Our results confirm that the adsorption process is predominantly driven by chemisorption, owing to the particular coordination between Fe(III) and amidoxime groups (—NH_2/—OH). The density of functional groups and pore structure are critical for regulating adsorption kinetics.[34] The adsorption rate is proportional to the square of the number of unoccupied active sites, which is consistent with the observed biphasic kinetics. It was also observed that K_2 decreased with increasing initial concentration and leveled off at approximately 100 mg·L^{-1} (Fig. 4c), which was attributed to the interplay between active site saturation and diffusion limitations.[35] As adsorption proceeded, the amidoxime groups on the Ami-gauze were gradually occupied, reducing the driving force for subsequent adsorption.

To ensure statistical rigor and address the limitations of linearization, a nonlinear first-order (Eq. 11) and second-order (Eq. 12) dynamic kinetic models[36] were also applied to characterize the adsorption behavior.

$$Q_t = Q_e \times \left(1 - e^{-k_1 t}\right) \tag{11}$$

$$\frac{t}{Q_t} = \frac{1}{Q_e} + k_2 \times t \tag{12}$$

where k_1 and k_2 are the adsorption rates of the corresponding kinetic models. The fittings of the experimental data using nonlinear first/second-order kinetic models are shown in Figs. 4(d) and 4(e), and the fitting parameters are listed in Table S2 (in ESI). The results indicate that the nonlinear second-order kinetic model provides a more accurate description of adsorption dynamics. These findings suggest that the adsorption process is complex and cannot be adequately described by simple linear models.

The adsorption process between the adsorbate in the solution and the surface of the adsorbent may be controlled by one or more steps, such as external diffusion, pore diffusion, surface diffusion, and adsorption on the pore surface.[37] To gain insight into the mechanisms and rate-controlling steps affecting the kinetics of adsorption, the experimental data were fitted using Weber's intra-particle diffusion equation (Eq. 13):[38]

$$Q_t = K_i t^{1/2} + A \tag{13}$$

where K_i is the intra-particle diffusion rate and A is the boundary layer thickness.[39] A larger A correlates with a larger contribution of surface sorption in the rate-controlling step. The plots of Q_t - $t^{1/2}$ can be depicted by two linear regimes (Fig. 4f), which suggests a two-step adsorption process. It is assumed that the external resistance to mass transfer surrounding the fibers of Ami-gauze is only significant in the early stages of adsorption, corresponding to the first sharper adsorption part. The second

linear regime is gradual adsorption dominated by intraparticle diffusion.[40] The intra-particle diffusion rate constants (K_i) and A are also listed in Table S3 (in ESI) along with the corresponding correlation coefficients (R^2). The constants of A were not zero, suggesting that pore diffusion was not the rate-limiting step. Obviously, K_{i1} is larger than K_{i2}, while A_1 is smaller than A_2. All the results show that the adsorption of Fe(III) over the Ami-gauze may be controlled by surface sorption followed by intra-particle diffusion mass transfer.

Adsorption Mechanism

FTIR and XPS analyses were performed before and after the adsorption experiments to investigate the Fe (III) capture mechanism of the Ami gauze. Fig. 5 shows the FTIR spectra of AOC, De-gauze, Ami-gauze, and Ami-gauze after adsorption of Fe(III) ions (Ami-gauze/Fe). The adsorption bands at 1660 cm^{-1} and 913 cm^{-1} in the FTIR spectrum of AOC correspond to C=N stretching and N—OH bending vibrations of the amidoxime groups,[41] respectively (Fig. 5a). The FTIR spectrum of the Ami-gauze exhibits an obvious C=N stretching vibration at 1687 cm^{-1} in addition to the C—OH vibration of cellulose at 1106 cm^{-1} (Fig. 5b). However, the relatively low loading of AOC resulted in weak peak intensities, leading to the absence of a discernible N—OH band. Furthermore, a distinct peak at 1715 cm^{-1} can be attributed to the C=O stretching vibration of the urethane linkage formed by the reaction between the hydroxyl groups on the cellulose backbone and the isocyanate functionalities of the cross-linker.[42] The FTIR results confirmed the successful immobilization of AOC onto De-gauze.

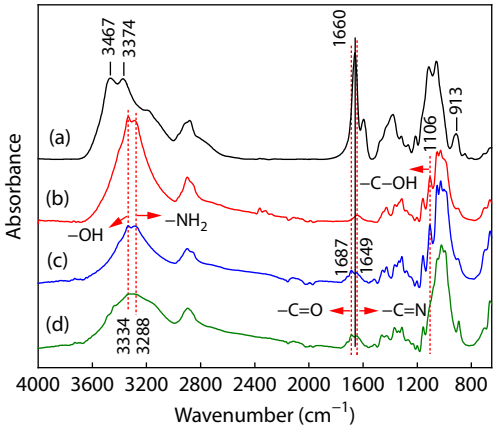

Fig. 5 FTIR spectra of (a) AOC, (b) De-gauze, (c) Ami-gauze, and (d) Ami-gauze/Fe.

Notable spectral changes were observed between the FTIR spectra of the Ami-gauze and Ami-gauze/Fe (Figs. 5c and 5d). The —OH and —NH_2 stretching vibration bands, initially located at 3334 and 3287 cm^{-1}, respectively, broadened and merged into a single broad envelope centered at 3327 cm^{-1} after the adsorption of Fe(III). This phenomenon can be explained by the formation of a coordination band between these groups and the Fe(III) ions. The oxygen atoms in the hydroxyl group and the nitrogen atoms in the amino group possess lone electron pairs, which can be donated to the vacant orbitals of the transition metal ions, Fe(III), resulting in electron density redistribution between the atoms.[43] Additionally, the disappearance of the C—O band at 1106 cm^{-1} and the red shift of the bands at 1158 and 1053 cm^{-1} to 1156 and 1050 cm^{-1} with reduced intensity suggest the coordination of Fe(III) ions with the oxygen atoms in the hydroxyl groups on the cellulose backbone.[44,45] However, the unchanged positions and intensities of the C=N band in the amidoxime group and the C=O band in PCL suggest that these groups are not involved in the coordination process.

The chemical states of the atoms involved in the adsorption process may change as a result of chemical interactions with the adsorbed species, which can be revealed by the XPS spectra.[46] Figs. 6(a)–6(c) are the XPS survey spectra of the De-gauze, Ami-gauze, and Ami-gauze/Fe. Compared with De-gauze, Ami-gauze shows a distinct N_{1s} peak in addition to the C_{1s} and O_{1s} peaks (Figs. 6a and 6b), which confirms the successful loading of AOC onto De-gauze. After the adsorption of Fe(III) ions, the spectrum demonstrated the emergence of an Fe_{2p} peak at 716.32 eV (Fig. 6j), providing direct evidence of the iron adsorption capability of the Ami-gauze.[47] The relatively weak intensity of the Fe_{2p} peak is attributed to the low content of adsorbed iron compared to that of the adsorbent. Figs. 6(d)–6(l) show detailed analyses of the high-resolution spectra of C_{1s}, O_{1s}, N_{1s}, and Fe_{2p}, and the fitting parameters are summarized in Table S4 (in ESI). The C_{1s} local spectra show new peaks at 289.08 and 289.60 eV, corresponding to the C atoms of —**C**=N—OH in the amidoxime group and —NH—**C**=O in the crosslinker (Fig. 6e). The N_{1s} local spectra show new peaks at 399.73, 400.84 and 401.98 eV, assigned to N atoms of —**N**H_2, —C=**N**—OH in amidoxime groups and O=C—**N**H— in the crosslinker (Fig. 6k). The results confirm the successful loading of AOC on the De-gauze. The local surface concentration of the amidoxime group was calculated to be 5.03 wt% (0.58 mmol·g^{-1}), far higher than the mass percentage (1.24%), proving surface adhesion. Furthermore, distinct peaks at 711.35 eV ($Fe_{2p,3/2}$) and 724.56 eV ($Fe_{2p,1/2}$), alongside the satellite peaks at 716.26 and 729.14 eV on the XPS spectra of Fe(III) adsorbed Ami-gauze (Fig. 6j), confirm that the chemisorption mediated by amidoxime-Fe(III) ions interaction of the coordination.[48,49] Comparison of the nitrogen (N) environments before and after adsorption (Figs. 6k and 6l) shows that the binding energies (BEs) shift to higher values. The peak representing the —**N**H_2 group shifts from 399.73 eV to 399.78 eV, while the peak assigned to the —**N**H—C=O group shifts from 401.90 eV to 401.98 eV. In contrast, the peak for the —C=**N** group shifts slightly from 400.86 eV to 400.84 eV. These shifts indicate a decrease in the electron density around the nitrogen atoms in the —**N**H_2 and —**N**H—C=O groups, whereas the nitrogen atom in the —C=**N** group experiences a reverse result.[50] Similarly, the analysis of the oxygen (O) environments (Figs. 6g–6i) shows observable shifts in BEs. The —C—**O**H peak shifts from 531.88 eV to 531.96 eV, and the peak assigned to the —N—**O**H group shifts from 532.69 eV to 532.74 eV.

Conversely, the peak for **O**=C—NH— shifts from 533.58 eV to 533.46 eV. These changes in BEs indicate that the nitrogen atoms in the —**N**H_2 and —**N**H—C=O groups and the oxygen atoms in the —C—**O**H and —N—**O**H groups directly participate in the coordination with Fe(III) ions.[51] The XPS and FTIR results confirm that the adsorption of Fe(III) ions by Ami-gauze primarily occurs *via* the formation of coordination bonds between Fe(III) ions and lone electron pairs on oxygen and nitrogen atoms. The key functional groups participating

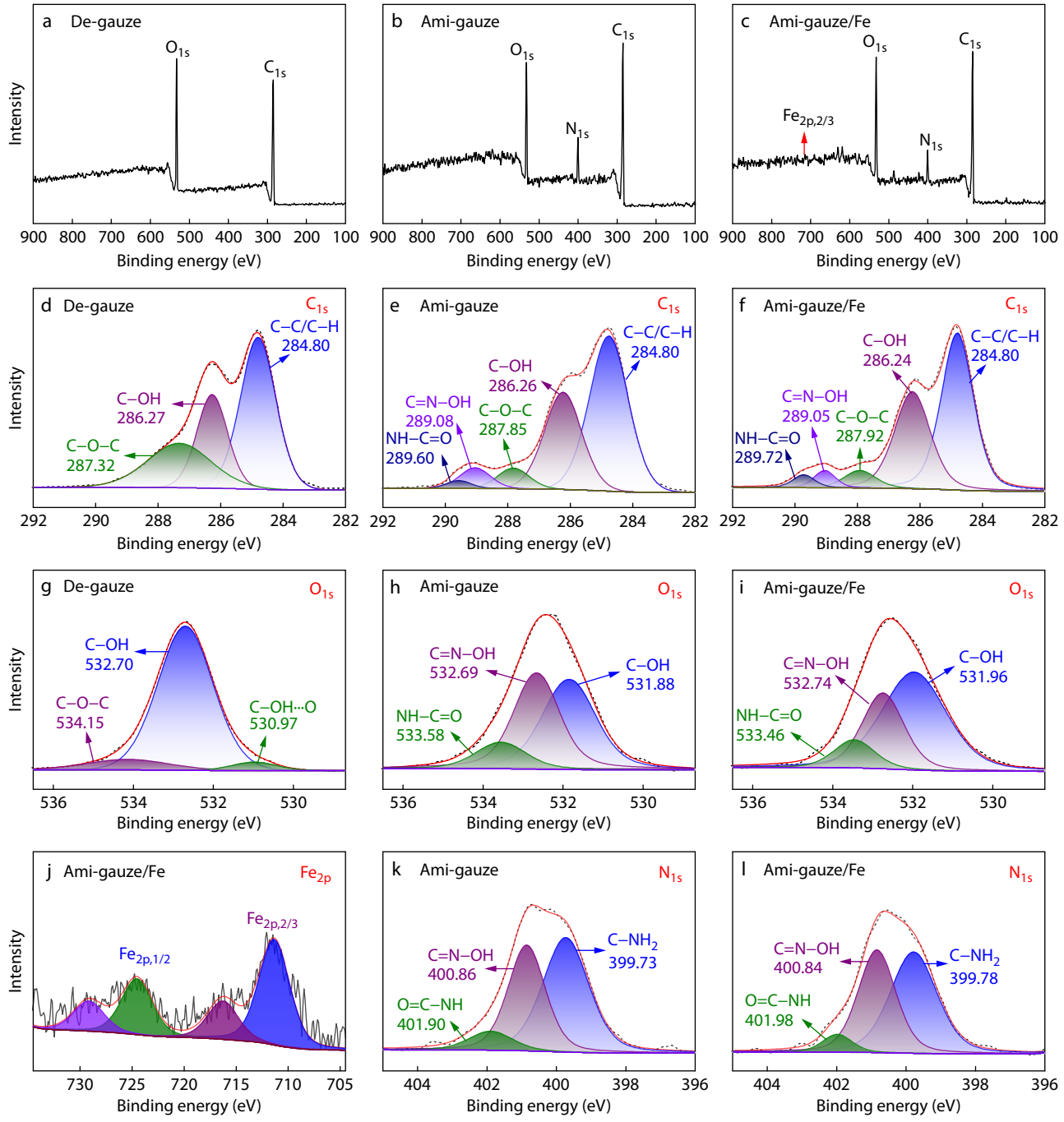

Fig. 6 XPS survey spectra (a–c); high-resolution XPS spectra of C_{1s} (d–f), O_{1s} (g–i), N_{1s} (k, l) of De-gauze, Ami-gauze, Ami-gauze/Fe, and Fe_{2p} (j) of Ami-gauze/Fe.

in the coordination included —**N**H_2, =N—**O**H, —C—**O**H, and —**N**H—C=O.[52] Therefore, Fe(III) adsorption onto Ami-gauze proceeds through multiple coordination pathways,[53] as depicted in Fig. 7. Among these possibilities, the hexacoordinate configuration in Fig. 7(a) may be the most prevalent, attributed to the thermodynamic favorability of the amidoxime group and the influence of steric hindrance, considering the high density of —OH groups. The participation of these active sites likely contributes to multilayer or heterogeneous adsorption, which aligns with the previously observed Freundlich-type adsorption behavior. Therefore, the inherent moisture function derived from hydrophilic cellulose networks and metal-chelating ability, mainly achieved by the coordination sites of amidoxime ligands, enables Ami-gauze to achieve simultaneous adsorption and effective fixation of iron ions.

Reactive and Reusable Properties of Ami-gauze

The reusability of an adsorbent is essential to its long-term feasibility and operational effectiveness.[54] Consequently, the feasibility of the Ami-gauze for cyclic applications was evaluated using multiple adsorption/desorption cycles. Fe(III) ions are easily

https://doi.org/10.1007/s10118-026-3679-5

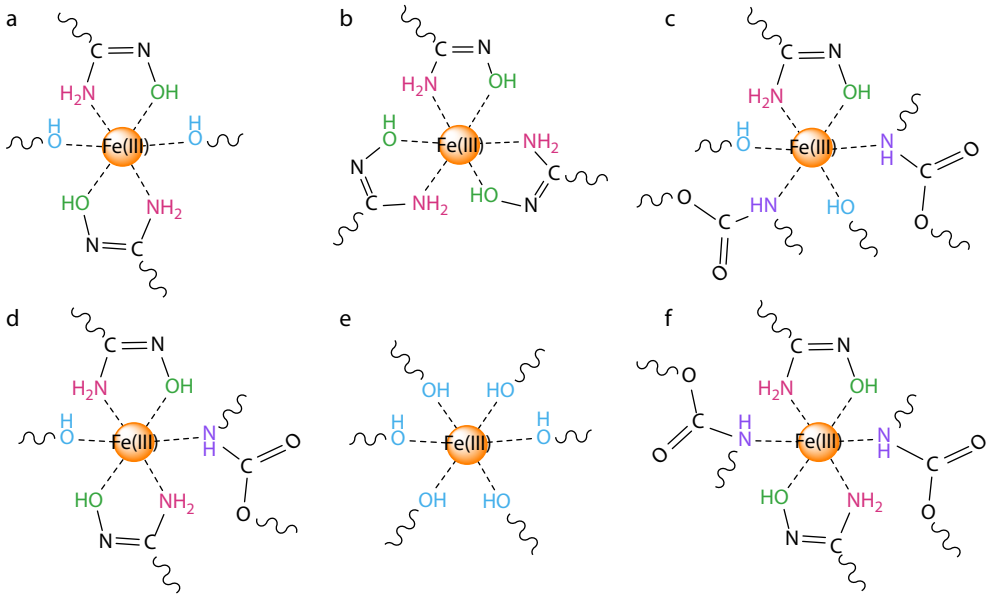

Fig. 7 Possible adsorption mechanism of Fe(III) on Ami-gauze with the coordination of (a) amidoxime group and cellulose backbone, (b) amidoxime group, (c, d) amidoxime group, cellulose backbone, and crosslinker, (e) cellulose backbone and (f) amidoxime group and crosslinker.

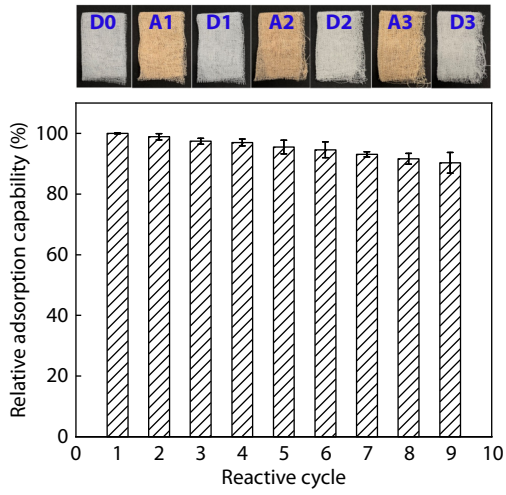

Fig. 8 The regeneration properties of Ami-gauze at the initial concentration of 20 mg·L^{-1} for the Fe(III) adsorption experiments. The inserted photos show the changes in color of Ami-gauze after the adsorption (**A1**–**A3**) and desorption (**D1**–**D3**).

desorbed from the Ami-gauze in saturated EDTA-2Na solution at room temperature. The photographs in Fig. 8 show that the color of Ami-gauze transitioned from orange-yellow to white during the first desorption cycle (**A1–D1**), and reverted to yellow upon re-exposure to the Fe(III) solution (**A2**). After nine cycles of treatment with Fe(III)/EDTA solutions, the color of the Ami-gauze gradually returned to its original state, indicating the effective removal of Fe(III) ions during each desorption process. Furthermore, the adsorption efficiency remained relatively stable even after repeated use, demonstrating the potential for sustainable and long-term application of the Ami-gauze.

In addition to visual observations, the concentration of iron ions during both the adsorption and desorption processes was quantitatively analyzed (Table S5 in ESI), and the adsorption efficiency versus regeneration cycles is shown in Fig. 8. A gradual decline in adsorption efficiency was observed with increasing reuse cycles, with the adsorption capacity of the Ami-gauze decreasing by 12.4% after nine cycles. The marginal efficiency decline in the Ami-gauze during cyclic operation originates from multiple mechanisms: (i) partially irreversible ion complexation, (ii) adsorbent matrix degradation during regeneration cycles, and (iii) residual species interference. Repeated washing/drying cycles induce physical degradation of the cellulose scaffold, compromising the structural integrity and causing partial detachment of amidoxime functionalities.[55] This reduces the effective surface area and active site density, thereby diminishing the Fe(III) adsorption capacity. Although EDTA effectively desorbs Fe(III) ions through competitive ligand exchange, residual Fe(III) may occupy coordination sites, while EDTA residues potentially modify the amidoxime group chemistry. Collectively, these factors reduced the chelating affinity of the amidoxime groups toward the target ions. These findings highlight the robust reusability of the Ami-gauze while underscoring the need for further optimization to minimize efficiency losses over extended use.

Furthermore, FTIR spectroscopy was performed on the Ami-gauze after each regeneration cycle. The FTIR results indicate that the stretching vibration bands of —OH, C—O, and —NH_2 groups at 3334, 1106, and 3287 cm^{-1} remained unchanged after nine cycles (Fig. S3 in ESI), which confirms the stability of the prepared cellulosic adsorbent materials. These results revealed that the structural changes that occur during the adsorption and desorption processes are reversible. The ability of the Ami-gauze to maintain its structural integrity and chemical stability during successive adsorption/desorption cycles highlights its durability and reusability, making it a promising candidate for scalable industrial applications.

Application of Ami-gauze on the Nanhai No. I Shipwreck

Ami-gauze was used to remove iron deposits from the marine archaeological wood selected from the Nanhai No. I shipwreck in the laboratory. Fig. 9 shows the adsorption efficiency of the

Ami-gauze at different application times and cycles. A comparative analysis of iron removal quantities by Ami-gauze applied for varying durations demonstrated that, as the application time increased, the amount of iron removed from waterlogged archaeological wood also increased. This finding indicates that the Ami-gauze had not yet reached adsorption equilibrium when attached to the marine archaeological wood. After eight adsorption/desorption cycles, the amount of iron removed from the wood using the same piece of Ami-gauze fluctuated but did not show a significant decrease, indicating that the Ami-gauze is reusable.

Ami-gauze was used *in situ* on the hull surface of the Nanhai I shipwreck. Photographs of both Ami-gauze samples during the application process, as well as those after iron deposit desorption, are presented in Fig. 10. The results indicate that the samples became brown after being attached to the hull surface for 4 days (Fig. 10a). After 48 days, these Ami-gauze became dark brown and indistinguishable from the attached hull (Fig. 10b). Ami-gauze can be recovered by desorption in the EDTA-2Na solution (Fig. 10c), and the faint residual tint may be introduced by the irreversible co-adsorption of wood-derived organics and stable iron-organic complexes. The amounts of iron desorbed from the gauze washed by the water and EDTA-2Na solution are listed in Table S6 (in ESI). The results confirmed that the Ami-gauze can effectively adsorb iron ions from the attached surface of the hull. The difference in the adsorbed amount could be attributed to the difference in the iron deposit content of the wood.

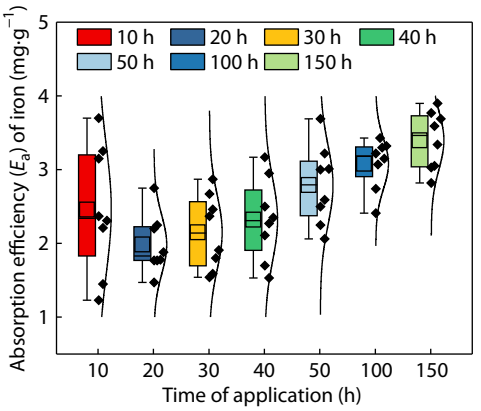

Fig. 9 Adsorbed iron content of Ami-gauze at different cycles.

Fig. 10 The photos of Ami-gauze after different attaching time of (a) 4 days and (b) 48 days on the Nanhai I shipwreck hull; (c) The samples after desorption.

CONCLUSIONS

This work presents a simple approach for preparing cost-effective and reusable Ami-gauze with exceptional adsorption performance for Fe(III) ions adsorption. Kinetic studies revealed that adsorption followed the pseudo-second-order model, suggesting a chemisorption-dominated mechanism. Isotherm analysis indicated that the adsorption process aligned more closely with the Freundlich isotherm model, which suggests the heterogeneous surface interactions and multilayer adsorption behavior due to the hierarchical pore structure and bidentate coordination capability of the amidoxime groups (—**N**H$_2$/=N—**O**H). The Ami-gauze showed promising reusability and retained over 87.6% of its adsorption capacity after nine adsorption-desorption cycles. The *in situ* experiments on the adsorption of iron ions from the hull surface of the Nanhai I shipwreck indicated that the Ami-gauze is efficient for the adsorption of iron ions. Our results confirmed that the amidoxime functionalized materials have promising applications in the conservation of marine waterlogged wooden artifacts, as well as in other fields for the adsorption of heavy metal ions at low cost.

Conflict of Interests

The authors declare no interest conflict.

Electronic Supplementary Information

Electronic supplementary information (ESI) is available free of charge in the online version of this article at http://doi.org/10.1007/s10118-026-3679-5.

Data Availability Statement

The data supporting the findings of this study are available from the corresponding author upon reasonable request.

ACKNOWLEDGMENTS

This work was financially supported by China's National Key R&D Program (No. 2020YFC1521802).

REFERENCES

1 Monachon, M.; Albelda-Berenguer, M.; Lombardo, T.; Cornet, E.; Moll-Dau, F.; Schramm, J.; Schmidt-Ott, K.; Joseph, E. Evaluation of an alternative biotreatment for the extraction of harmful iron and sulfur species from waterlogged wood. *Eur. Phys. J. Plus* **2021**, *136*, 937.
2 Fors, Y.; Jalilehvand, F.; Risberg, E. D.; Björdal, C.; Phillips, E.;

Graphical Abstract

Recyclable and Easy-to-apply Amidoxime Functionalized Cellulose for Continuous Removal of Iron Ions from Shipwreck Woods

Ting-Ting Zhang, Hong-Ying Zhang, Hong-Liang Kang, Da-Wa Shen, and Rui-Gang Liu

Institute of Chemistry, Chinese Academy of Sciences; China Academy of Cultural Heritage; Shaanxi University of Science & Technology; University of Chinese Academy of Sciences

A cost-effective and scalable amidoxime-functionalized gauze was developed to efficiently extract iron ions from marine wooden artifacts. Synergizing the hygroscopicity of gauze with the metal-binding affinity of amidoxime groups, this reusable cellulose adsorbent retains over 87.6% of its capacity after nine regeneration cycles, providing a practical solution to mitigate iron-induced degradation in cultural relics.

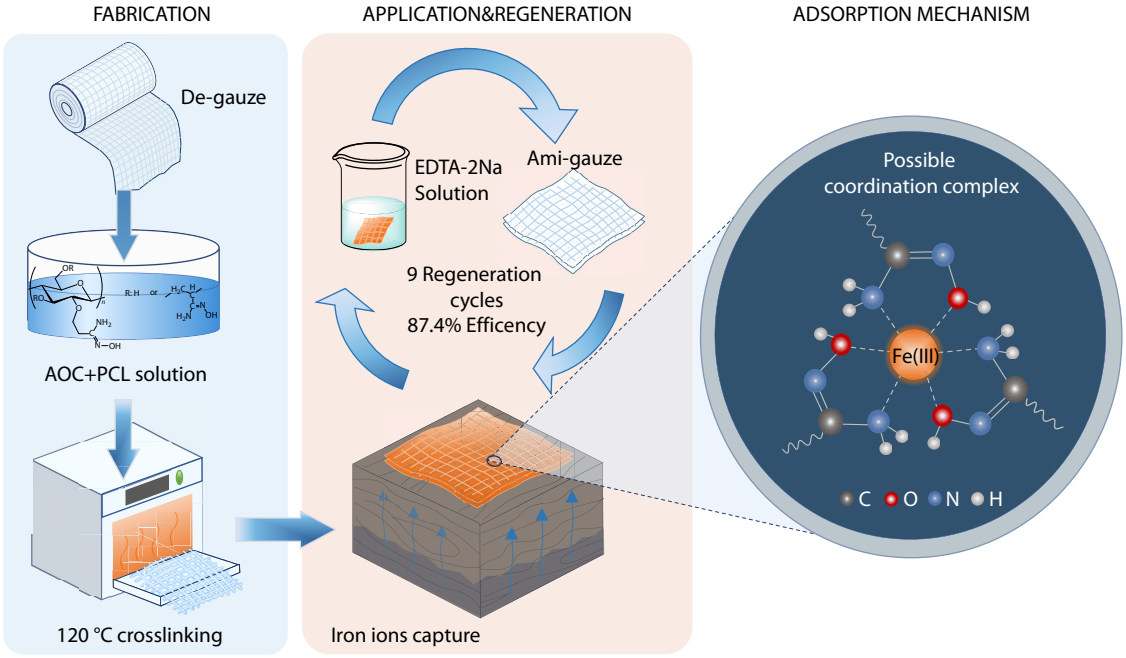

Chinese J. Polym. Sci. 2026, 44, 2607–2618 *https://doi.org/10.1007/s10118-026-3679-5*

Sandström, M. Sulfur and iron analyses of marine archaeological wood in shipwrecks from the Baltic Sea and Scandinavian waters. *J. Archaeol. Sci.* **2012**, *39*, 2521–2532.

3 Broda, M.; Hill, C. A. S. Conservation of waterlogged wood-past, present and future perspectives. *Forests* **2021**, *12*, 1193.

4 Shen, D. W.; Li, N. S.; Fu, Y.; Macchioni, N.; Sozzi, L.; Tian, X. L.; Liu, J. Study on wood preservation state of Chinese ancient shipwreck Huaguangjiao I. *J. Cult. Herit.* **2018**, *32*, 53–59.

5 Zhang, Z. G.; Li, N. S.; Tian, X. L.; Liu, J.; Shen, D. W. Research on the removal of the iron sulfides in the Qing Dynasty marine shipwreck, Ningbo Xiaobaijiao No. I. *Sciences of Conservation and Archaeology* **2014**, *26*, 30–38.

6 Shen, D. W., Sulfur-Iron Compounds in Marine Source-Derived Wooden Cultural Relics; Science Press: Beijing, **2020**.

7 Richards, V. in *Wet wood conservation colloquium - extended abstracts*, Upper Swabia, Germany, **2016**, pp. 39–43.

8 Jenssen, V. In *Conservation of Marine Archaeological Objects*; Pearson, C., Ed.; Butterworth-Heinemann: Oxford, **1987**, pp. 122–163.

9 Pelé, C.; Guilminot, E.; Labroche, S.; Lemoine, G.; Baron, G. Iron removal from waterlogged wood: Extraction by electrophoresis and chemical treatments. *Stud. Conserv.* **2015**, *60*, 155–171.

10 Zhang, H. Y.; Shen, D. W.; Zhang, Z. G.; Kang, H. L.; Ma, Q. L. Comparison of iron deposits removing material from the marine archaeological wood of Nanhai I shipwreck. *J. Cult. Herit.* **2024**, *66*, 59–67.

11 Li, J. Y.; Hu, Z. Y.; Zhang, S. D.; Zhang, H. S.; Guo, S. J.; Zhong, G. M.; Qiao, Y.; Peng, Z. Q.; Li, Y. T.; Chen, S. G.; Chen, G. H.; Cao, A. M. Molecular engineering of renewable cellulose biopolymers for solid-state battery electrolytes. *Nat. Sustain.* **2024**, *7*, 1481–1491.

12 Macior, A.; Zaborniak, I.; Wolski, K.; Spilarewicz, K.; Raczkowska, J.; Janiszewska, N.; Awsiuk, K.; Chmielarz, P. Synthesis of hydrophobic and antifouling wood-polymer materials through SI-ATRP: Exploring a versatile pathway for wood

functionalization. *ACS Appl. Polym. Mater.* **2024**, *6*, 11427–11443.
13 Riseh, R. S. Advancing agriculture through bioresource technology: The role of cellulose-based biodegradable mulches. *Int. J. Biol. Macromol.* **2024**, *255*, 128006.
14 Ani, P. C.; Nzereogu, P. U.; Agbogu, A. C.; Ezema, F. I.; Nwanya, A. C. Cellulose from waste materials for electrochemical energy storage applications: A review. *Appl. Surf. Sci. Adv.* **2022**, *11*, 100298.
15 Seddiqi, H.; Oliaei, E.; Honarkar, H.; Jin, J. F.; Geonzon, L. C.; Bacabac, R. G.; Klein-Nulend, J. Cellulose and its derivatives: towards biomedical applications. *Cellulose* **2021**, *28*, 1893–1931.
16 Jing, L. D.; Shi, T. Y.; Chang, Y. L.; Meng, X. L.; He, S.; Xu, H.; Yang, S. T.; Liu, J. Cellulose-based materials in environmental protection: A scientometric and visual analysis review. *Sci. Total Environ.* **2024**, *929*, 172576.
17 Zhang, P. B.; Lu, Y. D.; Fan, M. M.; Jiang, P. P.; Bao, Y. M.; Gao, X. W.; Xia, J. L. Role of cellulose-based composite materials in synergistic reinforcement of environmentally friendly waterborne polyurethane. *Prog. Org. Coat.* **2020**, *147*, 105811.
18 Li, W. W.; Liu, R. G.; Kang, H. L.; Sun, Y. M.; Dong, F. Y.; Huang, Y. Synthesis of amidoxime functionalized cellulose derivatives as a reducing agent and stabilizer for preparing gold nanoparticles. *Polym. Chem.* **2013**, *4*, 2556–2563.
19 Zhang, H. Y.; Shen, D. W.; Zhang, Z. G.; Ma, Q. L. Characterization of degradation and iron deposits of the wood of Nanhai I shipwreck. *Herit. Sci.* **2022**, *10*, 202.
20 Schindler, W. D.; Hauser, P. J. In *Chemical Finishing of Textiles*; Schindler, W. D.; Hauser, P. J., Eds.; Woodhead Publishing, **2004**, p. 7–28.
21 Berns, R. S., in *Billmeyer and Saltzman's Principles of Color Technology* (4th ed.) John Wiley & Sons, **2019**, p. 272.
22 Cui, W. R.; Zhao, Q. Q.; Lin, X. H.; Liu, S.; Li, Y. B.; Cai, C. S. Regenerable and stable olefin-linked covalent organic frameworks with coordination template for selective and efficient trapping of scandium ion. *Appl. Surf. Sci.* **2025**, *681*, 161590.
23 He, X. L.; Deng, H. C.; Wu, H.; Yu, W.; Guo, Z. M.; Liang, X. M. Amidoxime-based polymer microspheres with high selectivity for uranium from saline lake brine. *ACS Appl. Polym. Mater.* **2023**, *5*, 4380–4387.
24 Li, H. Y.; Chen, S. C.; Huang, H. J.; Fang, Y.; Weng, Y. X.; Chen, Q. H.; Liu, X. Q.; Liu, H. Q. Modified cotton gauze with high hemostatic efficacy due to controllable hygroscopicity and wet tissue adhesiveness. *J. Appl. Polym. Sci.* **2024**, *141*, e55861.
25 Wasilewska, M.; Derylo-Marczewska, A.; Marczewski, A. W. Comprehensive studies of adsorption equilibrium and kinetics for selected aromatic organic compounds on activated carbon. *Molecules* **2024**, *29*, 2038.
26 Sheikhmali, M.; Jalilnejad, E.; Rafiee, R. Synthesis, characterization, experimental design and process analysis of heavy metals adsorption on a wheat straw based amidoximated bioadsorbent. *Sci. Rep.* **2024**, *14*, 31083.
27 Han, C. L.; Cao, M. M.; Yu, J.; Wang, S. T.; Zhou, X. L.; Chen, Y. H.; Yang, F. Carboxymethyl cellulose-based composite polymer hydrogels cross-linked with epichlorohydrin and application for Cu(II) Removal. *ACS Appl. Polym. Mater.* **2023**, *5*, 2070–2078.
28 Foo, K. Y.; Hameed, B. H. Insights into the modeling of adsorption isotherm systems. *Chem. Eng. J.* **2010**, *156*, 2–10.
29 Langmuir, I. The adsorption of gases on plane surfaces of glass, mica and platinum. *J. Am. Chem. Soc.* **1918**, *40*, 1361–1403.
30 Chu, K. H. Revisiting the Temkin isotherm: Dimensional inconsistency and approximate forms. *Ind. Eng. Chem. Res.* **2021**, *60*, 13140–13147.
31 Freundlich, H. Über die Adsorption in Lösungen. *Z. Phys. Chem.* **1907**, *57U*, 385–470.
32 Tawfik, A. M.; Eltabey, R. M. Fractional kinetic strategy toward the adsorption of organic dyes: Finding a way out of the dilemma relating to pseudo-first- and pseudo-second-order rate laws. *J. Phys. Chem. A* **2024**, *128*, 1063–1073.
33 Ho, Y. S.; McKay, G. Pseudo-second order model for sorption processes. *Process Biochem.* **1999**, *34*, 451–465.
34 Yang, W. J.; Wu, D. C.; Fu, R. W. Porous structure and liquid-phase adsorption properties of activated carbon aerogels. *J. Appl. Polym. Sci.* **2007**, *106*, 2775–2779.
35 Aita, S. A.; Mahmoud, R.; Hafez, S. H. M.; Zaher, A. Investigating adsorption of aqueous heavy metals through isotherms and kinetics with Zn-Co-Fe/LDH for remarkable removal efficiency. *Appl. Water Sci.* **2025**, *15*, 75.
36 Largitte, L.; Pasquier, R. A review of the kinetics adsorption models and their application to the adsorption of lead by an activated carbon. *Chem. Eng. Res. Des.* **2016**, *109*, 495–504.
37 Hu, Q. L.; Ma, S. T.; He, Z. H.; Liu, H. Y.; Pei, X. J. A revisit on intraparticle diffusion models with analytical solutions: Underlying assumption, application scope and solving method. *J. Water Process. Eng.* **2024**, *60*, 105241.
38 Weber, W. J.; Morris, J. C. Kinetics of adsorption on carbon from solution. *J. Sanit. Eng. Div.* **1963**, *89*, 31–59.
39 Hameed, B. H.; Mahmoud, D. K.; Ahmad, A. L. Equilibrium modeling and kinetic studies on the adsorption of basic dye by a low-cost adsorbent: Coconut (*Cocos nucifera*) bunch waste. *J. Hazard. Mater.* **2008**, *158*, 65–72.
40 Han, R. P.; Zhang, L. J.; Song, C.; Zhang, M. M.; Zhu, H. M.; Zhang, L. J. Characterization of modified wheat straw, kinetic and equilibrium study about copper ion and methylene blue adsorption in batch mode. *Carbohydr. Polym.* **2010**, *79*, 1140–1149.
41 Li, W. Q.; Yuan, H. Y.; Wang, P. Y.; Zhai, S. R.; Ma, J. L.; Wang, Y.; Xiao, J. Q.; Shen, Y.; Guo, H. Amidoxime-functionalized corn straw for efficient Cr(VI) adsorption from water: Waste utilization, affinity character and DFT simulation. *Colloid Surf. A-Physicochem. Eng. Asp.* **2024**, *689*, 133631.
42 Mira-Cuenca, C.; Meslier, T.; Roig-Sanchez, S.; Laromaine, A.; Roig, A. Patterning bacterial cellulose films with iron oxide nanoparticles and magnetic resonance imaging monitoring. *ACS Appl. Polym. Mater.* **2021**, *3*, 4959–4965.
43 Wang, F.; Zhang, Y. K.; Li, Y. P.; Chen, B. Amidoxime-functionalized carboxymethylcellulose based porous hydrogels adsorbent fabricated from oyster shell stabilized Pickering emulsions for enhanced adsorption of Gd^{3+} and Er^{3+}. *Int. J. Biol. Macromol.* **2025**, *307*, 141962.
44 Yang, H.; Liu, J. K.; Wu, W. J.; Luo, Y. Q.; Mo, G. H.; Huang, K. Synthesis of amidoxime-modified hollow organic porous nanospheres for efficient uranium adsorption from aqueous solution. *ChemistrySelect* **2023**, *8*, e202301214.
45 Zhang, Y. H.; Jiang, X. Q.; Wang, J.; Yu, J.; Zhang, Y.; Wu, W. S.; Xin, S.; Sheng, X. L. Fabrication of chitosan-based multifunctional supramolecular hydrogel for efficient wood preservation. *ACS Appl. Polym. Mater.* **2025**, *7*, 17154–17163.
46 Greczynski, G.; Haasch, R. T.; Hellgren, N.; Lewin, E.; Hultman, L. X-ray photoelectron spectroscopy of thin films. *Nat. Rev. Method. Prim.* **2023**, *3*, 40.
47 Graat, P. C. J.; Somers, M. A. J. Simultaneous determination of composition and thickness of thin iron-oxide films from XPS Fe 2p spectra. *Appl. Surf. Sci.* **1996**, *100*, 36v40.
48 Yamashita, T.; Hayes, P. Analysis of XPS spectra of Fe^{2+} and Fe^{3+} ions in oxide materials. *Appl. Surf. Sci.* **2008**, *254*, 2441–2449.
49 Biesinger, M. C.; Payne, B. P.; Grosvenor, A. P.; Lau, L. W. M.; Gerson, A. R.; Smart, R. S. Resolving surface chemical states in XPS analysis of first row transition metals, oxides and hydroxides: Cr, Mn, Fe, Co and Ni. *Appl. Surf. Sci.* **2011**, *257*, 2717–2730.

50 Zhang, W. Q.; Liu, C.; Meng, X. R.; Sun, J.; Tian, H. Y. A green and low-cost preparation of polyacrylonitrile fibers with imine dioxime and amidoxime groups for efficient and selective gold recovery. *Chem. Eng. J.* **2024**, *489*, 151246.
51 Shi, N.; Wu, J. K.; Zhi, X. Y.; Li, N.; Wang, Z. N. Amidoxime-functionalized cellulose nanofibers/MXene aerogel for electric field enhanced uranium extraction from seawater. *Chem. Eng. J.* **2023**, *476*, 146563.
52 Luo, D.; Hu, S. Z.; Huang, T.; Zhang, N.; Lei, Y. Z.; Wang, Y. Electrospun cellulose acetate/polyethylenimine porous fibers toward highly efficient removal of Cr(VI). *ACS Appl. Polym. Mater.* **2022**, *4*, 7945−7957.
53 Walsh, Z.; Janecek, E. R.; Hodgkinson, J. T.; Sedlmair, J.; Koutsioubas, A.; Spring, D. R.; Welch, M.; Hirschmugl, C. J.; Toprakcioglu, C.; Nitschke, J. R.; Jones, M.; Scherman, O. A. Multifunctional supramolecular polymer networks as next-generation consolidants for archaeological wood conservation. *Proc. Natl. Acad. Sci. U. S. A.* **2014**, *111*, 17743−17748.
54 Al-aizari, F. A.; Thamer, B. M.; Hameed, M. M. A.; Al-Enizi, A. M.; El-Newehy, M. H. Novel functionalized poly(ethylene-*co*-vinyl alcohol) as a high-performance adsorbent for cationic dyes in wastewater treatment. *J. Appl. Polym. Sci.* **2025**, *142*, e57379.
55 Schlapp-Hackl, I.; Rissanen, M.; Ojha, K.; Sawada, D.; Gorniak, K.; Onkinen, E.; Niinimäki, K.; Sixta, H. From postconsumer cotton towels to new cotton textile fibers. *J. Appl. Polym. Sci.* **2024**, *141*, e55460.

https://doi.org/10.1007/s10118-026-3679-5